# Modeling the Behavior of an Electronically Switchable Directional Antenna for Wireless Sensor Networks

Biruk Silase Geletu

February 10, 2011

SICS Technical Report T2011:04
ISSN 1100-3154

This thesis is presented as part of the degree of Master of Science in Electrical Engineering

Blekinge Institute of Technology


Swedish Institute of Computer Science

Swedish Institute of Computer Science | SICS

| | | | |
|---|---|---|---|
| Supervisor: | Luca Mottola, | Ph.D. | Swedish Institute of Computer Science |
| Examiner: | Jörgen Nordberg, | Ph.D. | Blekinge Institue of Technology |

**Dedication**

In loving memory of my mom

**Acknowledgements**

I have worked on this master thesis with the Network Embedded Systems (NES) Group of the Swedish Institute of Computer Science (SICS) at Kista, Stockholm. I would like to take the opportunity to thank all the people in the group for all the important discussions we have had during my stay.

I would like to express my deep and sincere gratitude to my supervisor, Luca Mottola (Ph.D.), for his coaching, guidance, support and inspiration. It has been a privilege to work with him and to get the time that he has taken to comment on my works. The coaching and the inspiration that I have got from him would mean a lot to me in my future carrier. I would like to express my gratitude to the manager of the NES group, Thiemo Voigt (Ph.D.), for his timely suggestions, support and understanding. I would like to thank a post-doctoral researcher at SICS and my office mate, Simon Duquennoy (Ph.D.), who has always been willing to share me from his expertise in different tools whenever I asked him.

I am grateful for the follow up, suggestions, feedbacks and advice that I have got from the thesis coordinator and my examiner at Blekinge Institute of Technology (BTH), Jörgen Nordberg (Ph.D.). His timely suggestions and encouragement have been a very good motivation for me.

Finally, I would like to appreciate the love, support and company of my family especially my dad.

This work was financed by VINNOVA, the Swedish Agency for Innovation Systems, and the Uppsala VINN Excellence Center for Wireless Sensor Networks WISENET.

**List of Abbreviations**

| | |
|---|---|
| ADC | Analog to Digital Converters |
| API | Application Program Interface |
| DAas | Directional Antenna at Sink |
| DirC-MAC | Directional Contention MAC |
| DtD MAC | Directional to Directional MAC |
| ECU | Electronic Control Unit |
| ESPE | Electronically Switched Parasitic Element |
| FBPA | Four Beam Patch Antenna |
| GPS | Global Positioning System |
| IDC | Insulation Displacement Connector |
| IDDA | Interest Dissemination with Directional Antenna |
| ISM | Industrial, Scientific and Medical |
| I/O | Input-Output |
| LAN | Local Area Networks |
| LQI | Link Quality Indicator |
| MAC | Media Access Control |
| OSI | Open Systems Interconnection |
| PAN | Personal Area Networks |
| PDF | Probability Density Function |
| PRR | Packet Reception Rate |
| QoS | Quality of Service |
| RF | Radio Frequency |
| RISC | Reduced Instruction Set Computing |
| RSSI | Received Signal Strength Indicator |
| SICS | Swedish Institute of Computer Science |
| SMA | SubMiniature version A |
| SPI | Serial Peripheral Interface |
| SPIDA | SICS Parasitic Interference Directional Antenna |
| S-MAC | Studio MAC |
| TCP/IP | Transmission Control Protocol/ Internet Protocol |
| USB | Universal Serial Bus |
| WAN | Wide Area Networks |
| WSN | Wireless Sensor Networks |

# Contents

# List of Figures

# List of Tables

**Abstract**

Reducing power consumption is among the top concerns in Wireless Sensor Networks, as the lifetime of a Wireless Sensor Network depends on its power consumption. Directional antennas help achieve this goal contrary to the commonly used omnidirectional antennas that radiate electromagnetic power equally in all directions, by concentrating the radiated electromagnetic power only in particular directions. This enables increased communication range at no additional energy cost and reduces contention on the wireless medium.

The SPIDA (SICS Parasitic Interference Directional Antenna) prototype is one of the few real-world prototypes of electronically switchable directional antennas for Wireless Sensor Networks. However, building several prototypes of SPIDA and conducting real-world experiments using them may be expensive and impractical. Modeling SPIDA based on real-world experiments avoids the expenses incurred by enabling simulation of large networks equipped with SPIDA. Such a model would then allow researchers to develop new algorithms and protocols that take advantage of the provided directional communication on existing Wireless Sensor Network simulators.

In this thesis, a model of SPIDA for Wireless Sensor Networks is built based on thoroughly designed real-world experiments. The thesis builds a probabilistic model that accounts for variations in measurements, imperfections in the prototype construction, and fluctuations in experimental settings that affect the values of the measured metrics. The model can be integrated into existing Wireless Sensor Network simulators to foster the research of new algorithms and protocols that take advantage of directional communication. The model returns the values of signal strength and packet reception rate from a node equipped with SPIDA at a certain point in space given the two-dimensional distance coordinates of the point and the configuration of SPIDA as inputs.

**Keywords:**
Wireless Sensor Networks, Directional Antennas, Non-parametric Probability Density Function Estimation, Spatial Interpolation

# Chapter 1

# Introduction

The convergence of the Internet and wireless communication coupled with recent advances in engineering is paving the way for the exciting technology of Wireless Sensor Networks (WSNs). WSNs consist of tiny devices with severe resource constraints in energy, bandwidth, processing power and memory. This poses several challenges for researchers engaged in the field.

Most of the available devices in WSNs are equipped with omnidirectional antennas. Omnidirectional antennas radiate electromagnetic power equally in all directions. Directional antennas have appeared as beneficial in saving energy and improving communication reliability in WSNs. They radiate the electromagnetic power only in particular directions enabling increased communication range at no additional energy cost and protecting the radiated power from obstacles and interference in other directions. Lots of work have been done in studying the effects of using directional antennas in WSNs. Most of these works are solely based on simulations. Only very few works have tried to design practical directional antennas for WSNs.

SPIDA (SICS Parasitic Interference Directional Antenna) is an electronically switchable directional antenna designed based on a previously existing SPIDA prototype design [17, 18]. The latest work also presents preliminary measurements from SPIDA in real-world settings with their improvement over the widely used omnidirectional antennas in WSNs.

This thesis builds a model of SPIDA for WSNs. The model is built based on extensive real-world experiments with an adequate number of devices. The model returns the values of signal strength and packet reception rate from a base node equipped with SPIDA at a certain point as outputs given the two-dimensional distance coordinates of the point and the configuration of SPIDA as inputs. The modeling methods apply random variable theory to account for temporal variations in the metrics considered, imperfections in the prototype construction and fluctuations in experimental settings that affect the values of the measured metrics. The spatial variation of the metrics is also modeled with a suitable two-dimensional interpolation mechanism.

## 1.1 Problem Statement

Two of the most important issues in WSNs are reducing power consumption without affecting reliability in communication and mitigating the limitations of the wireless communication medium. SPIDA increases communication range without any additional energy cost and improves performance in WSNs. This is achieved by concentrating the radiated electromagnetic power only in particular directions instead of radiating the power equally in all directions.

There is only one prototype of SPIDA and that is the one designed at SICS. It would be expensive and very challenging to build several prototypes of SPIDA and perform real-world experiments using them together with a large number of nodes. Thus, modeling SPIDA for WSNs saves the costs incurred and the challenges involved. The model can then be integrated into existing WSN simulators to foster further researches.

Much of the intellectual effort in this thesis lies in designing suitable real-world experiments in a practical WSN equipped with SPIDA. The main difficulties are designing the appropriate experiments with available software and hardware, tackling the temporal and spatial variations in the metrics considered, identifying different factors affecting experimental results and accounting for them. Much intellectual effort has been put in building an accurate model that accounts for the associated variations and factors.

## 1.2 Method

In this thesis experimental studies in real-world settings are used to build the model. The appropriate experiments are designed with available software and hardware. The appropriate environment for the experiments is carefully selected. The results of the experiments are attested through several repetitions in the relevant experimental setups to serve as the building blocks of the model. Two major problems are observed in the process of building the model:

- temporal variations in the measured metrics
- large spread distance between the points where we measure the metrics giving rise to a large spatial variation in the measured metrics

In this thesis random variable theory is applied to study the randomness observed in the temporal variation of the measured metrics. The methods from random variable theory also account for imperfections in the prototype construction and fluctuations in experimental settings that affect the values of the measured metrics. A suitable two-dimensional spatial interpolation mechanism is used to add fictitious points between the real points and estimate the values of the metrics at these points thus increasing the spatial granularity of the collected data.

## 1.3 Alternative Approaches

To build a model of SPIDA for WSNs, two of the metrics measured in this thesis are the signal strength and the packet reception rate at different points in a two-dimensional space. The standard two-antenna method of measuring the field strength from an antenna can be used to determine the signal strength at different points [1]. This widely used method among antenna design professionals involves measuring the received power or open-circuit voltage developed in a standard receiving antenna by the field to be measured. Using this method, the field strength from the antenna is computed from the measured voltage and the dimensions and form of the standard antenna.

This is a complex method requiring the use of several sophisticated devices and equipments. Besides that, the method does not provide a quantitative measure of the packet reception rate. But the software and hardware used in this thesis measure both the signal strength and the packet reception rate at different points in a two-dimensional space.

## 1.4 Research Contributions

This thesis provides the first model of an electronically switchable directional antenna for WSNs based on extensive real-world experiments. The model returns the values of signal strength and packet reception rate from a base node equipped with SPIDA at a certain point as outputs given the two-dimensional distance coordinates of the point and the configuration of SPIDA as inputs. The built model will have several benefits for existing and future researches in WSNs using SPIDA. The model can be integrated into existing WSN simulators. Researchers can then use the model in developing different routing and MAC protocols that take advantage of directional communication without the need to perform practical measurements using SPIDA. Researches on localization and neighbor discovery can also be done in an effective manner with the provided model. The integration of the model with simulators has also an additional benefit since there is no limit on the number of nodes in a simulator.

## 1.5 Thesis Structure

The remaining part of the thesis is structured as follows. Chapter 2 gives background information on wireless communication, WSNs and antennas. Besides that, the chapter also discusses related works in directional antennas for WSNs and gives background information on random variable theory, density estimation and two-dimensional spatial interpolation. Chapter 3 starts by informing the goal of the experiments and proceeds to describe the hardware used and the program written to perform experiments. The chapter ends after briefly describing the setup of the experiments. Chapter 4 starts by describing the different experiments performed. It also presents summarized results from representative experimental settings. The procedures followed in building the model, a sample model data and the model use are presented in chapter 5 together with

the experimental data used for modeling. The thesis is concluded in chapter 6 together with suggestions for future work.

# Chapter 2

# Background

Wireless communication has become the most exciting area in communications and networking. Smart environments represent the next evolutionary development step in buildings, industries, homes, and transportation systems. The information needed by smart environments is provided by WSNs which are responsible for sensing, processing and communication. A WSN is typically characterized by the temporal and spatial dynamics of its metrics that are associated with the wireless communication link such as the signal strength and packet reception rate. The temporal and spatial dynamics of these metrics in a WSN can be modeled using techniques from random variable theory and spatial interpolation. Random variable theory can be used to estimate the likely values of a quantity whose measured values show uncertainty. Spatial interpolation is used to estimate the values of a quantity at different points in space where actual measurements of the quantity are not taken.

## 2.1 The Wireless Domain

The introduction and growth of new applications of wireless communication in recent years has generated tremendous researches and changes in communication and networking. WSNs are among the new applications of wireless communication with low power. Modern WSNs are made up of a large number of inexpensive devices that are networked via low power wireless communication. It is the networking capability that fundamentally differentiates a WSN from a mere collection of sensors, by enabling cooperation, coordination and collaboration among sensor assets. Harvesting advances in the past decade in microelectronics, sensing, analog and digital signal processing, wireless communication and networking, WSN technology is expected to have a significant impact in our lives in the twenty-first century.

### 2.1.1 Wireless Communication

Wireless communication allows us to exchange information over a certain distance without the use of electrical conductors or wires. Wireless data networks, cellular net-

works, satellite television, cordless telephones, Global Positioning System (GPS) units and WSNs recently are among the different wireless systems common in the modern society. Wireless communication is the best candidate in situations where areas cannot be covered by typical cabling and in cases of moving workstations. The infrared, microwave and radio frequencies can all be used for wireless communication. The radio frequencies (RFs) are frequently used in typical applications including wireless data networks and WSNs. Different standards included in the IEEE802 are adopted and used worldwide for wireless communication.

Different wireless data networks including Personal Area Networks (PANs), Local Area Networks (LANs), Metropolitan Area Networks (MANs) and Wide Area Networks (WANs) are integral parts of our society these days. All wireless networks including WSNs whether big or small have a certain structure common to all. They basically communicate by means of formatted units of data known as *packets* in the commonly used packet switching technique for communication between nodes [23]. A packet consists of two kinds of data: control information and user data. The control information contains the necessary details for a proper delivery of the user data. These include source address, destination address and error detection codes. The different activities in the network are arranged in a hierarchical order as in the TCP/IP and OSI protocol stacks to ensure a reliable delivery of the packets [23].

A typical wireless communication scenario involves a transmitter, a receiver and a medium of propagation which is in reality a complex environment consisting of many obstacles [7]. The transmitter modulates a carrier according to the input message to be transmitted and radiates the output as a propagating wave by its antenna. The receiver converts the propagating wave collected by its antenna with the interference from the environment to a useful signal that approximates the input signal. RF transceivers are designed to operate at certain frequencies depending on the different applications and network specific standards that are adopted for wireless communication.

The radio link between the transmitter and the receiver is an integral part of wireless communication. An RF communication involves modulation, bandpass filtering, demodulation and multiplexing circuits. Different radio chip sets with all the mentioned functionality are produced and integrated into different wireless networks including WSNs. Radios must detect signals of widely varying magnitude in the presence of interfering devices. A radio is also required to minimize excess noise while tolerating large input signals without excessive distortion [7].

The performance of a wireless communication system is highly influenced by the medium of propagation. In empty space, the transmitted power decreases inversely with the square of the distance between the transmitter and receiver. Even in an open field with flat terrain, there is reflection of waves by the ground. Additionally, scattering and diffraction contribute to the path loss of the transmitted power with distance. The *isotropic path loss* is the ratio of the total radiated power from the transmitting antenna to the power available at the receiver antenna. Ranges of different exponents

are determined to relate the inverse of the path loss known as path gain to distance for different physical environments [7]. The path gain (PG) is expressed as:

$$PG = k\left(\frac{d_0}{d}\right)^n \tag{2.1}$$

where $PG$ is the path gain, $d_0$ is the reference distance, $d$ is any distance, $k$ is the path gain when $d = d_0$, and $n$ is an exponent ranging from 2 for free space to 6 for obstructed buildings.

Interference is one of the bottlenecks in wireless communication. Interference is caused by the interaction of propagating waves that have approximately the same frequencies [3]. Interference can be *constructive* or *destructive* depending on the phase difference between the interacting waves. Constructive interference between two waves that are in-phase causes their amplitudes to add up when the waves interact. Destructive interference between two waves that are completely out of phase by $180^\circ$ causes the waves to cancel out each other during their interaction [3].

In our surrounding outdoor and indoor environments there are several impediments to wireless communication in addition to interference from other radios. These include reflection, scattering, diffraction and absorption of the propagating wave by buildings, people, cars and the ground. Due to that, the signal at the receiver has different components traveling over multiple paths. This results in variation of signal strength, frequency distortion, delay, and replication in the received wave in addition to the mix with other interfering signals and hence the unreliability of wireless links [7]. This is commonly known as *multipath fading*. Different fading models are built to determine the signal strength margin needed to ensure that reliable communication can be achieved at a certain probability.

### 2.1.2 Antennas in Wireless Communication

Antennas radiate the electromagnetic power that carries information in wireless communication. The power radiated by an antenna is usually shown in a three-dimensional space by a radiation pattern in its surrounding area. The radiation power pattern is usually plotted in decibels (dB). Two-dimensional cross-sections of the three-dimensional radiation patterns are also commonly used.

Antennas are produced in different sizes and shapes according to their specific applications. Each of these different antenna types have their own radiation characteristics. The most common ones are wire, microstrip (patch), array, reflector and aperture antennas [3]. Wire antennas can appear in different shapes such as straight wire, loop and helix. The straight wire antennas appear as dipoles and monopoles. The dipoles are further classified depending on their length in relation to the length of the waves they propagate. The quarter wavelength monopole is a widely used antenna with a mounting above a ground plane [3]. Microstrip antennas are low profile, inexpensive antennas which can be fabricated using modern printed-circuit technology. They can be mounted on different electronic devices. An array antenna is an aggregate of radiating elements

arranged to maximize radiation in a specific direction [3]. Yagi-Uda is a common array antenna. Reflector antennas are antennas with large dimensions used for communication over very large distances. The parabolic reflector is a common example of reflector antennas. Aperture antennas are sophisticated high frequency antennas used for special applications. They appear in the form of waveguide apertures and horns [3]. Cantenna is a common directional waveguide antenna used in long range WiFi. Figure 2.1 is a simple sketch showing the shapes of the common antenna types.

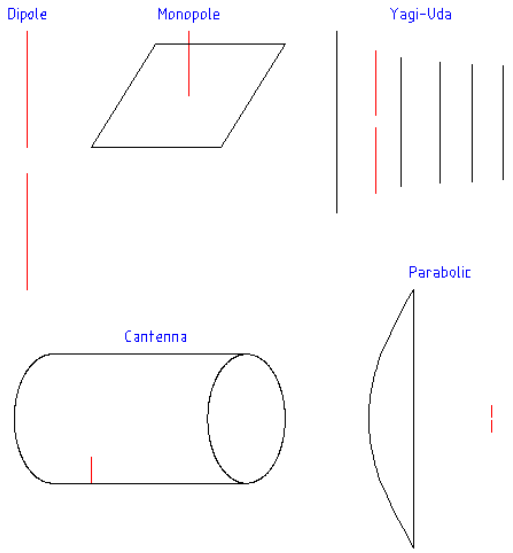


Figure 2.1: Common types of antennas

Antennas can broadly be classified as *directional* and *nondirectional* depending on the characteristics of their radiation pattern.

### Nondirectional Antennas

The ideal isotropic antennas which are not used in practice have a uniform spherical three-dimensional radiation pattern that corresponds to a nondirectional behavior. All other antennas have a nonuniform radiation pattern. The commonly used omnidirectional antennas have a directional behavior in the elevation plane and a nondirectional behavior in the azimuthal plane. They are usually considered as nondirectional due to their behavior in the azimuthal plane corresponding to a circular radiation pattern in two dimensions. Figure 2.2 shows the three-dimensional radiation patterns of isotropic and omnidirectional antennas and the corresponding two-dimensional cross-sections.

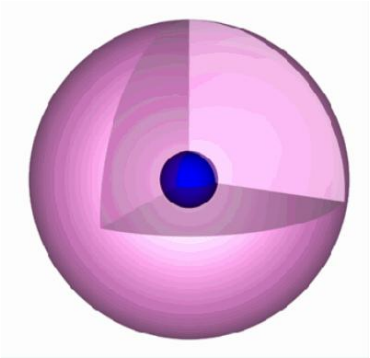

(a) Three dimensional radiation pattern of an isotropic antenna

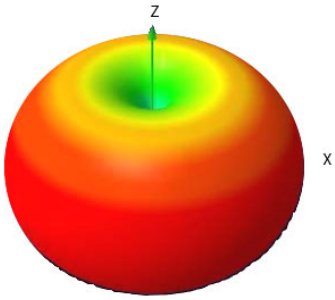


(b) Three dimensional radiation pattern of an omnidirectional antenna

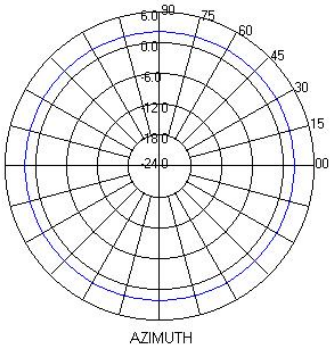


(c) Azimuthal plane cross section of the radiation pattern of an omnidirectional antenna

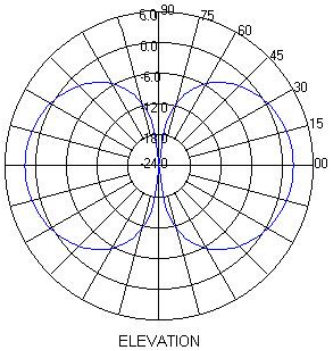


(d) Elevation plane cross section of the radiation pattern of an omnidirectional antenna

Figure 2.2: Radiation patterns of isotropic and omnidirectional antennas

### Directional Antennas

Arrays of different antenna elements can be configured in a specific geometrical and electrical arrangement to yield maximum radiation in a particular direction and minimum or no radiation in other directions. This is made possible by a constructive interference of the radiated fields from the array elements in the desired direction and a destructive interference in other directions [3]. The resulting *directional antennas* radiate the electromagnetic beam much more in that direction compared to the other directions [3]. This increases communication range at no additional energy cost. The harmful effects of multipath fading can also be mitigated by using directional antennas since we can direct narrow beams to the intended directions there by protecting the radiated power from obstacles and interference in other directions [14]. The same reasoning also allows for higher signal to interference ratios [14]. The two-dimensional radiation pattern of a directional antenna is shown in Figure 2.3. Directional antennas

are usually larger in size compared to their nondirectional counterparts. There are three basic constructions of directional antennas:

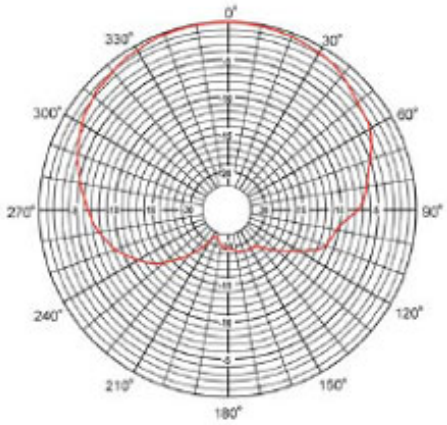


Figure 2.3: Radiation pattern of a directional antenna

1. **Fixed single-beam directional antennas**: The arrangement of the elements results in a single beam that concentrates the radiation in a particular direction. The sectoral array that is used for mobile communication and the Yagi-Uda array are typical examples of this category. The fixed single-beam directional antennas need a physical alteration to change the direction of maximum radiation without any phase shift difference between the excitation currents of the different array elements [3]. Many of these constructions are bulky and not suitable for WSNs.

2. **Switched multiple-beam directional antennas**: Their construction allows them to choose from one of predefined radiation beams covering different regions of space [3]. The only practical and feasible switched multiple-beam directional antennas that are constructed for WSNs are SPIDA and the four-beam patch antenna [18, 17, 13]. Both of these directional antennas have a moderate size that makes them suitable for WSNs. The recent version of SPIDA is an electronically switchable directional antenna that gives the possibility of directing different radiation beams from its six legs covering different regions in space without any physical alteration [18].

3. **Smart antennas**: They can dynamically adjust the radiation pattern to enhance reception while minimizing interference using signal-processing algorithms [3]. Since they are generally more digital-processing intensive and require a radio behind each antenna element, they are more expensive than switched-beam systems [3]. Their complexity and cost make them impractical for WSNs.

### 2.1.3 Wireless Sensor Networks (WSNs)

A WSN is a collection of spatially distributed autonomous sensor nodes that can cooperatively monitor different physical or environmental conditions and obtain data [2, 27]. A WSN is usually left unattended after its deployment. The development of WSNs was motivated by military applications such as battlefield surveillance, battle damage assessment and targeting. Currently WSNs are employed in various environmental, health, industrial and home applications.

Figure 2.4 shows an application example of monitoring volcanic eruptions with a WSN deployed on Volcan Tungurahua, an active volcano in Ecuador [24]. The network is based on the Mica2 sensor platform that consists of three infrasonic (low-frequency acoustic) microphone nodes. The nodes first transmit data to an aggregation node that sends the data over a 9 km wireless link to a laptop at the volcano observatory. A separate GPS receiver establishes a common time base for the infrasonic sensors.

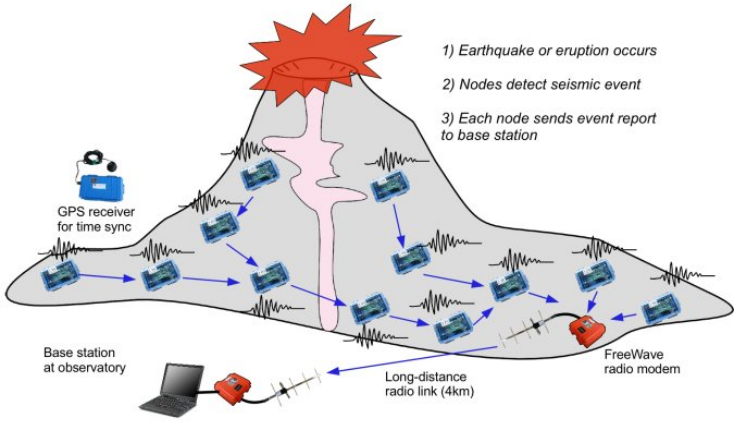


Figure 2.4: Monitoring volcanic eruptions with a WSN [24]

The development of smart sensor nodes in recent years has tremendously increased the popularity of WSNs. The smartness of the recent sensor nodes lies in their data processing capability along-side their communication capability compared to the previously existing sensors. Smart sensor nodes are low-cost, low-power, small-size, multifunctional devices that have the potential to communicate effectively within short distances [2]. A large number of sensor nodes is usually deployed in a small area. The density can range from few sensor nodes to few hundred sensor nodes in a region which can be less than 10m in diameter [9]. A wireless sensor node basically consists of four different components as shown in Figure 2.5: a sensor, a processor with a limited memory, a wireless communication interface and a power storage.

Different mechanical, seismic, volcanic, thermal, humidity, visual, biological, acoustic, chemical, optical and magnetic sensors can be attached to a sensor node to measure

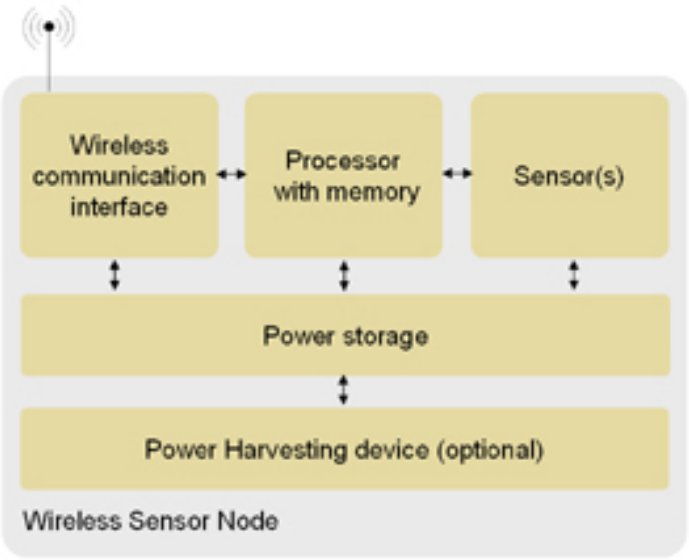


Figure 2.5: Block diagram of a typical wireless sensor node

various properties of the environment [27]. The sensors in a smart sensor node are equipped with a signal conditioning unit and analog to digital converters(ADCs). The digital electrical signals produced according to the sensed quantity are then fed into the processor. The processor together with the associated small memory controls the collaboration between the different nodes in a network. Different microcontrolles with a flash memory are built and integrated to wireless sensor nodes to serve as processors. Operating systems are designed by researchers that run on sensor nodes and help us to interact with the nodes. The nodes are normally powered by batteries which may be supported by power harvesting devices such as solar cells.

The wireless communication interface with its radio transceiver connects the node to the network. WSNs require a small sized, low-cost, ultra-low power transceiver. The industrial, scientific and medical (ISM) band of frequencies are commonly used in WSNs. The path loss between two sensor nodes may be as high as the fourth exponent of the distance between them i.e $n = 4$ in (2.1). This is because the antennas of the sensor nodes are close to the ground [20]. However, RF communication is still preferred in WSNs due to the small packet size, low data rate and high frequency reuse allowed by short range communication distances. Multihop communication is also commonly used in WSNs to save energy since communication using many short-range hops saves more energy compared to few long-range hops.

Protocol stacks are developed for power efficient communication, delivery of packets and collaboration between sensor nodes in a WSN. The protocol stacks combine power and routing awareness and integrate data with networking protocols [2]. The protocol

stack consists of the application, transport, network, data link and physical layers combined with power management, mobility management and task management planes as shown in Figure 2.6. Different types of application software are built and used at the application layer depending on the sensing tasks. The transport layer helps to maintain the flow of data especially when the WSN is to be accessed through the Internet or other external networks. The network layer controls the routing of the data from the transport layer. The Medium Access Control (MAC) Protocol at the data link layer minimizes packet collisions in a noisy environment with awareness of power constraints to ensure reliable communication. The physical layer addresses the needs of a simple but robust modulation, transmission and receiving techniques. The three planes coordinate the sensing task and lower the overall power consumption.

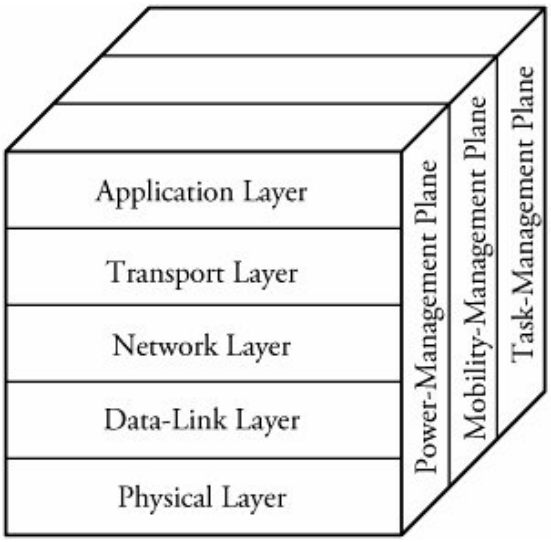


Figure 2.6: WSN protocol stack [2]

All the subunits of a smart wireless sensor node are expected to fit into a module having the size of a matchbox [15]. There are certain other stringent constraints on sensor nodes in addition to the size requirement [16]. The nodes must:

- consume extremely low power
- operate in high volumetric densities
- have low production cost
- be adaptive to the environment

Power has been such an important requirement in wireless sensor nodes due to their inaccessibility. The size limitations have also their share on the importance of the power

requirement. Sensor nodes carry limited, usually irreplaceable power sources. Hence the life time of a WSN depends on the life time of the power resources of the nodes [2]. Contrary to traditional networks that focus on providing high quality of service (QoS), WSN protocols and researches primarily focus on power conservation. The power of a sensor node is basically consumed by its three main activities: sensing, communication and data processing. Of the three domains, a sensor node expends maximum energy in data communication involving both data transmission and reception [2]. This is the fact that has made for the largely unexplored open research issues in decreasing power expenditures at the physical layer with a reliable communication. The use of directional antennas in the transceiver appears here as a possible solution.

### 2.1.4 Directional Antennas in WSNs

The possible advantages of directional antennas initiated researchers to work in designing MAC and routing protocols that use directional antennas for WSNs and other related networks such as wireless ad-hoc networks [5, 26, 11, 25, 8, 22, 12, 13, 18]. Most of the aforementioned works are based on simulations and analytical models of directional antennas for WSNs. The results from these works have shown that directional communication in WSNs that is provided by directional antennas results in:

- increased communication range of the nodes at no additional energy cost
- less contention in the network
- improved power consumption
- increased network life time
- improved throughput
- lower delay
- lessening the harmful effects of multipath fading
- increasing the signal to interference ratio

Santivanez et al. [5] focus on analyzing significant issues of contention based MACs for directional antennas in sensor networks and provide a MAC design that overcomes the difficulties. Wu et al. [25] introduce a directional-antenna-assisted reactive routing protocol, Interest Dissemination with Directional Antenna (IDDA), for WSNs. They show that IDDA enhances energy efficiency, packet delivery ratio, and target detection ratio in a target detection application. Cho et al. [8] propose mounting a directional antenna at the sink node in a WSN. They show that Directional Antenna at Sink (DAaS) increases network life time. DAaS is accompanied by a sink beam pattern scheduling algorithm that coordinates MAC layer wakeup/sleep schedules of the sink and the neighbor nodes according to the beam pattern schedule of the directional antenna. Shihab et al. [22] propose a directional-to-directional (DtD) MAC protocol for

ad-hoc networks. They show that DtD MAC improves network throughput in ad-hoc networks.

Dunlop et al. [11] introduce the use of switched beam directional antennas in WSNs. The resulting simulations show a reduction of interference, transmission delay and flooding consequently improving throughput and energy consumption in comparison to an existing solution based on S-MAC protocol. Dunlop et al. [12] investigate the introduction of switched beam directional antennas in WSNs using a synchronized sleep/awake contention-based MAC (DirC-MAC) protocol. The resulting simulations show improvements in throughput, delay and power consumption. Yago et al. [26] present a new distributed energy-efficient multicast protocol with directional antenna incorporating localized tree reconfiguration procedure for wireless ad-hoc networks. The resulting simulations show improvements in throughput and power consumption.

Giorgetti et al. [13] present one of the few works that show in-field practical experiments conducted on WSNs using an early switched beam directional antenna prototype. They design the four beam patch antenna (FBPA) shown in Figure 2.7 and integrate it with COTS motes. FBPA operates in the 2.4 GHz ISM band with IEEE 802.15.4 standard. They show that FBPA extends the communication range from 140m to 350m outdoors and reduces signal variability by 70%. FBPA also exhibits interference suppression from IEEE 802.11g systems.

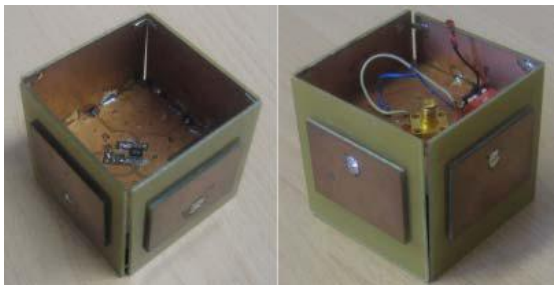

Figure 2.7: Top views of four beam patch antenna [13]

Nilsson [17] describes three classical types of directional antennas: the adcock-pair antenna, the pseudo-doppler antenna, and the electronically switched parasitic element antenna. He further adds that the last type is the most suitable for WSNs and presents the early design details and beam pattern measurements of the prototype electronically controllable switched-beam directional antenna for 2.4 GHz ISM band: SPIDA. SPIDA, which is shown in Figure 2.8 connected to a Tmote Sky sensor node, is originally designed for localization purposes in WSNs. SPIDA is smaller in size compared to FBPA.

Öström et al. [18] build a version of SPIDA that interfaces to the Tmote Sky sensor node at SICS. They design and implement the software drivers necessary to dynamically control the direction of maximum gain. They further evaluate the performance

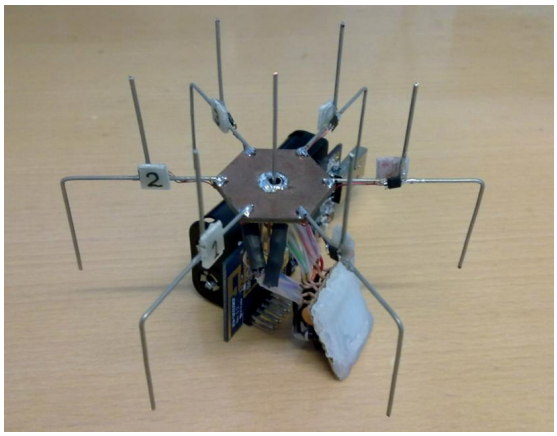


Figure 2.8: SPIDA prototype connected to a Tmote Sky node [18]

of the SPIDA prototype in real-world settings in comparison with two omnidirectional antennas: the on-board microstrip antenna and an external whip antenna for WiFi networks. They also point to network-level mechanisms that can implement the SPIDA and benefit from it. They show that by using SPIDA:

- communication range can be increased at no additional energy cost
- more stable performance can be achieved compared to mainstream antennas
- better correspondence between link performance and common link quality estimators can be observed

This thesis sets apart from most of the work done in the area in different aspects. First, it is one of the few works that are carried out based on real-world experiments using an electronically switchable directional antenna. Second, the work in this thesis is based on a practical synthetic setup of a WSN distributed in space and equipped with SPIDA, producing a model that fully characterizes an electronically switchable directional antenna for WSNs. The metrics considered in this thesis, the setup of the experiments, and the probabilistic model produced distinguish it from all the related works.

## 2.2 Random Variables

A random variable is a function of the elements of a sample space $S$ [19]. Given an experiment defined by a sample space $S$ with elements $s$, we assign to every $s$ a real number $X(s)$ according to some rule and call $X(s)$ a random variable. A discrete random variable can take only discrete values. A continuous random variable has a continuous range of values. It is also produced from a continuous sample space. The probability of occurrence of any discrete value of a continuous random variable

is zero. The random variable concept is scientifically feasible for modeling in cases where certain randomness is observed in the outcomes of an experiment. The cumulative distribution function and probability density functions are the two fundamental functions that are used to characterize a random variable [19]. The probability density function gives the likelihood that the random variable takes a certain value [19].

Different random variables exhibit different shapes of probability density functions characterized by certain parameters. The mean or average and standard deviation are the most common parameters involved in different density functions along with the associated mathematical expression [19]. Gaussian (normal), uniform, Poisson, binomial, exponential and Rayleigh distributions are among the most common density functions. The density function of a random variable can be estimated in two ways based on a finite collected data sample: *parametric* and *non-parametric* [4].

### 2.2.1 Parametric Methods of Density Estimation

These methods assume a specific functional form of the density function among one of the known density functions and adjust the parameters of the density function to fit the data [4]. These methods provide the best estimate when the probability density that the data follows is known as a priori. Their drawback is that the particular form of parametric density function may be incapable of providing a good representation of the true density [4].

Here, the probability density function $p(x)$ is represented in terms of specific functional form which contains a number of adjustable parameters [4]. The values of the parameters are then optimized to give the best fit to the data. The simplest and widely used parametric density model is the Gaussian distribution with its convenient analytical and statistical properties.

There are two principal approaches used to determine the values of the parameters from the data in parametric density estimation: *maximum likelihood method* and *Bayesian inference* [4]. These two approaches can lead to similar results but their conceptual base is different. Maximum likelihood seeks to find the optimum values for the parameters by maximizing a likelihood function derived from the data. However, in the Bayesian approach the parameters themselves are described by a probability distribution [4].

#### Maximum Likelihood Method

This method starts by assuming a density function $p(x)$ which depends on a set of parameters $\Theta = \{\theta_1, ..., \theta_M\}$ and a dataset of $N$ values $X = \{x_1, ..., x_N\}$ [4]. To make the dependence on the parameters explicit, the density function can be written in the form $p(x|\Theta)$. If the values are drawn independently from the distribution $p(x|\Theta)$, then the joint probability density of the whole data set $X$ is given by:

$$p(x|\Theta) = \prod_{n=1}^{N} p(x_n|\Theta) \equiv L(\Theta) \tag{2.2}$$

where $L(\Theta)$ can be viewed as a function of $\Theta$ for fixed $X$ [4]. $L(\Theta)$ is called the likelihood of $\Theta$ for the given $X$ [4]. The maximum likelihood method then sets the value of $\Theta$ by maximizing $L(\Theta)$. This method is intuitive in that it chooses the $\Theta$ which is most likely to give rise to the observed data. It is practically more convenient to find the negative logarithm of the likelihood function:

$$E = -\ln L(\Theta) = -\sum_{n=1}^{N} \ln p(x_n|\Theta) \tag{2.3}$$

and to find a minimum of E [4].

**Bayesian Inference**

In the Bayesian inference method we describe the parameters by a *prior* probability density before we observe the data [4]. The prior probability density reflects that we have little idea of what values the parameters should take. Baye's theorem is then used to determine the corresponding *posterior* probability density after observing the data. The consistency of some values of the parameters with the data implies that the posterior distribution is narrower than the prior distribution.

The desired density function of an outcome $x$, given the data set $X$, can be written as an integral over a joint distribution [4]:

$$p(x|X) = \int p(x, \Theta|X)\, d\Theta \tag{2.4}$$

The integrand can be expanded using Baye's theorem of conditional probability as:

$$p(x, \Theta|X) = p(x|\Theta, X)p(\Theta|X) \tag{2.5}$$

The first factor however is independent of $X$ since it is the assumed form of parametrized density. It is completely specified once the values of the parameters $\Theta$ have been set [4]. Hence we have:

$$p(x|X) = \int p(x|\Theta)p(\Theta|X)\, d\Theta \tag{2.6}$$

Thus, the Bayesian approach performs a weighted average over all values of $\Theta$ instead of choosing a specific value for $\Theta$. The weighting factor $p(\Theta|X)$, which is the posterior distribution of $\Theta$, is determined by starting from some assumed prior distribution $p(\Theta)$ and then updating it using Baye's theorem to take account of the data set $X$ [4]. Since the data points $\{x_1, ..., x_N\}$ are assumed to be drawn independently from the same underlying distribution, we can write:

$$p(X|\Theta) = \prod_{n=1}^{N} p(x_n|\Theta) \tag{2.7}$$

which is exactly the likelihood function introduced in (2.2).

The posterior distribution for $\Theta$ can then be written in the form:

$$p(\Theta|X) = \frac{p(X|\Theta)p(\Theta)}{p(X)} = \frac{p(\Theta)}{p(X)} \prod_{n=1}^{N} p(x_n|\Theta) \tag{2.8}$$

where the normalization factor in the denominator is given by:

$$p(X) = \int p(\Theta') \prod_{n=1}^{N} p(x_n|\Theta')\, d\Theta' \tag{2.9}$$

The evaluation of integrals such as (2.9) and (2.6) is very complex to perform and it is only analytically feasible for the class of density functions for which the posterior density in (2.7) has the same functional form as the prior.

### 2.2.2 Nonparametric Methods of Density Estimation

In nonparametric methods of density estimation we want to model the probability density which generated the data without making any prior assumption about the form of the density. Hence, these methods make fewer assumptions and the probability density function is estimated from the collected data itself [4]. *Histogram* and *kernel based estimation* are the most common nonparametric methods.

#### Histogram

The histogram is a simple yet practical method of density estimation. The histogram is obtained by dividing the axis of the data $x$ into a number of bins, and approximating the density at each value of $x$ by the fraction of points which fall inside the corresponding bin [4]. The histogram suffers from severe limitations to be applied in practical situations. Its major limitations are discontinuities at the boundaries of the bins, and its deviation from the true structure of density functions [4].

#### Kernel based estimation

The probability that a value $x$ drawn from an unknown density function $p(x)$ will fall inside some region $R$ of the $x$ axis is by definition given as [4]:

$$P = \int_R p(x')\, dx' \tag{2.10}$$

If there are $N$ data points drawn independently from $p(x)$ then the probability that $K$ of them will fall within the region $R$ can be approximated as below [4]:

$$P \approx \frac{K}{N} \tag{2.11}$$

Assuming that $p(x)$ is continuous and does not vary appreciably over the region $R$, (2.10) can be approximated by:

$$P = p(x)l \tag{2.12}$$

where $l$ is the length of the region $R$ and $x$ is some point lying inside $R$ [4].

The intuitive result below can be determined from (2.11) and (2.12) [4]:

$$p(x) \approx \frac{K}{Nl} \tag{2.13}$$

The kernel based density estimation techniques fix the length $l$ and determine $K$ from the data to obtain an estimate of the density function. It is expected that in the limit of an infinite number of data points, the estimation procedure becomes exact [4]. The kernel function $H(u)$ that corresponds to a square of area unity at the origin is defined as below [4]:

$$H(u) = \begin{cases} 1, & |u| < \frac{1}{2} \\ 0, & \text{otherwise} \end{cases} \tag{2.14}$$

Thus, for all data points $x_n$, the quantity $H(\frac{(x-x_n)}{l})$ is equal to unity if the point $x_n$ falls inside a region of length $l$ centered on $x$ and is zero otherwise. The total number of points falling inside the region can be simply expressed as below [4]:

$$K = \sum_{n=1}^{N} H(\frac{x - x_n}{l}) \tag{2.15}$$

Substituting (2.15) in (2.13), the estimate below can be determined for the density at point $x$ [4]:

$$\tilde{p}(x) = \frac{1}{N} \sum_{n=1}^{N} \frac{1}{l} H(\frac{x - x_n}{l}) \tag{2.16}$$

The discontinuities in the estimate can be smoothed out by using different forms of the kernel function $H(u)$. Considering the common choice normal kernel for smoothing, the density estimate is expressed as follows [4]:

$$\tilde{p}(x) = \frac{1}{N} \sum_{n=1}^{N} \frac{1}{\sqrt{2\pi l^2}} exp\{-\frac{(x - x_n)^2}{2l^2}\} \tag{2.17}$$

Figure 2.9 visualizes the construction of a kernel density estimate of 10 points using the normal kernel.

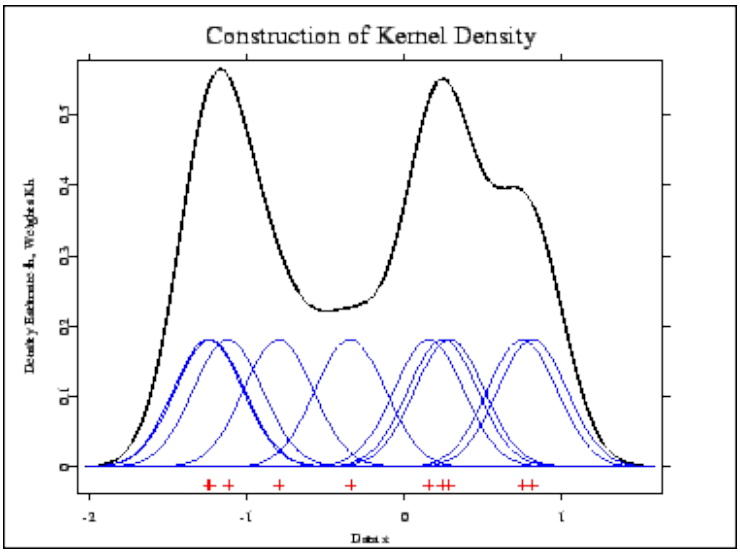


Figure 2.9: Kernel density estimate as a sum of bumps

There is no definite information on the probability density that the metrics considered in this thesis follow. Hence the parametric methods of density estimation are not used in this thesis. Nevertheless, the nonparametric method of density estimation based on kernel estimation is used in a similar but different problem for WSNs [6]. Hence, the nonparametric methods of density estimation are used in the modeling part of this thesis.

## 2.3 Two-dimensional Spatial Interpolation

Spatial interpolation is the process of using measured data values at particular locations to estimate the values of the data at locations where actual measurements cannot be taken. The acquisition of the new data values involves two stages: the creation of new locations and estimation of the data values at those new locations [21]. There are three common methods to estimate the data value at the new locations: *nearest neighbor interpolation*, *bilinear interpolation* and *spline interpolation*. All of these two-dimensional spatial interpolation mechanisms are commonly employed to increase the number of pixels of an image in image processing [21].

### 2.3.1 Nearest Neighbor Interpolation

This is the simplest method of two-dimensional interpolation. In order to estimate the data value at any location in the overlay grid, we look for the closest location in the original grid and assign its data value to the location in the grid [21]. This method has a large mean square error and it is not applicable in cases where accuracy is a

requirement.

### 2.3.2 Bilinear Interpolation

Bilinear interpolation is a general-purpose two-dimensional interpolation mechanism based on four neighbors [21]. It is equivalent to applying linear interpolation first in the horizontal direction and then in the vertical direction. Assuming a function $f$ having different values at the four corners of the square region shown in Figure 2.10, the value at an arbitrary location $(x, y)$ inside the region can be found from the equation below [21]:

$$\begin{aligned} f(x,y) =& (x_2 - x)(y_2 - y)f(x_1, y_1) + (x - x_1)(y_2 - y)f(x_2, y_1) \\ &+ (x_2 - x)(y - y_1)f(x_1, y_2) + (x - x_1)(y - y_1)f(x_2, y_2) \end{aligned} \tag{2.18}$$

Hence the function can be modeled in two dimensions as below [21]:

$$f(x, y) = ax + by + cxy + d \tag{2.19}$$

where $a, b, c$ and $d$ are coefficients determined from the values of the function at the four corners.

### 2.3.3 Spline Interpolation

The spline interpolation methods use more than four neighbors for interpolation. Using more points implies fitting the points with a more complex surface the simplest of which is a bicubic surface. This generally gives smoother results. These methods require complex computations and they are also difficult to implement.

Due to its error proneness, the nearest neighbor interpolation method is ruled out in this thesis. The associated extra computation and implementation burden of spline interpolation is also not justifiable for a general-purpose spatial interpolation problem such as the one in this thesis [21]. Hence, bilinear interpolation is chosen to perform a two-dimensional spatial interpolation on the metrics considered in this thesis.

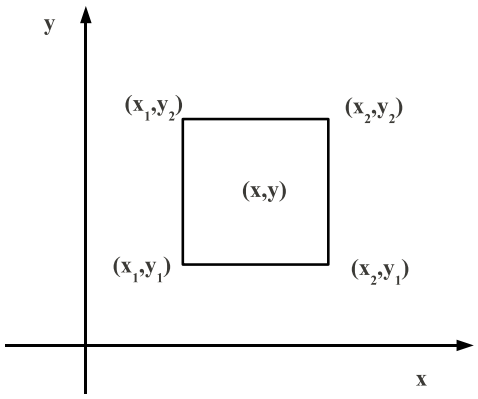


Figure 2.10: Region for performing bilinear interpolation

# Chapter 3

# Methodology

A set of experiments based on a synthetic setup of a WSN are designed and implemented to obtain useful data for building a model of SPIDA for WSNs in this thesis. The suitable software and hardware are selected to conduct the experiments. Appropriate values are selected for the input parameters within the experiment program to reduce the effect of temporary fluctuations in the environment and obtain a more accurate model. An environment with minimum disturbances and interferences is also selected targeting the accuracy of the model.

## 3.1 Goal of Experiments

The main aim of the experiments conducted in this thesis is to develop a model of SPIDA for WSNs based on real experimental data. This is achieved by first measuring the values of selected output metrics corresponding to specific values of selected input metrics. The nodes are placed systematically at different points in space. The model gives the values of signal strength and packet reception rate from a base node equipped with SPIDA at a certain point as outputs given the two-dimensional distance coordinates of the point and the configuration of SPIDA as inputs.

## 3.2 Hardware Used

Here two of the principal hardware used in this thesis are described: *the Tmote Sky sensor node* and *SPIDA*.

### 3.2.1 Tmote Sky Node

The Tmote Sky wireless sensor node is one of the most commonly used platforms in the WSN community. It can easily be reconfigured for an external SMA connected antenna such as SPIDA. It has an on-board USB connector which is used to program it from a PC using the supported operating system. It supports both of the widely used WSN operating systems: Contiki and Tiny OS. Contiki [10] is the operating system used in

this thesis. Because of the aforementioned reasons, the Tmote Sky platform is selected for the experiments in this thesis. The main components of the Tmote Sky Node are described briefly below as compiled from the Tmote Sky Datasheet [1]. Figure 3.1 shows the Tmote Sky node.

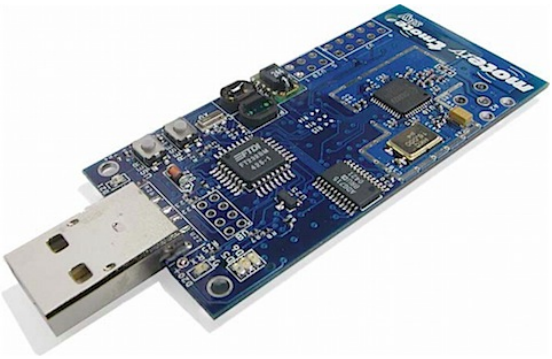

Figure 3.1: Tmote Sky node

**Power**

Tmote Sky is powered by two AA batteries. It is designed to operate in the range 2.1-3.6V DC. However the voltage must be at least 2.7V when programming the microcontroller flash or external flash. No battery is needed if a Tmote Sky is connected to the USB port for programming or communication. In this case the operating voltage is exactly 3V.

**Microprocessor**

Tmote Sky uses the ultra low power Texas Instruments MSP430 F1611 microcontroller with 10kB of RAM, 48kB of flash, and 128B of information storage. MSP430 F1611 microcontroller is a 16 bit RISC processor with extremely low active and sleep current consumption. The details of MSP430 F1611 are available in its datasheet [2].

**Radio**

Tmote Sky uses the Chipcon CC2420 radio chipset for wireless communication. The CC2420 is a low-power and IEEE 802.15.4 compliant radio. It can send up to 250 kbps. It is controlled by the MSP430 microcontroller through the SPI port, a series of digital input-output lines and interrupts. CC2420 can be shut off by the microcontroller for low power, duty cycled operations. It has also a programmable output power. The power levels and their corresponding dBm values, and the current consumption are

[1] http://www.bandwavetech.com/download/tmote-sky-datasheet.pdf
[2] http://www.chipcatalog.com/TI/MSP430F1611.htm

| Power Level | Output Power (dBm) | Current Consumption (mA) |
|---|---|---|
| 31 | 0 | 17.4 |
| 27 | -1 | 16.5 |
| 23 | -3 | 15.2 |
| 19 | -5 | 13.9 |
| 15 | -7 | 12.5 |
| 11 | -10 | 11.2 |
| 7 | -15 | 9.9 |
| 3 | -25 | 8.5 |

Table 3.1: Output power configuration for the CC2420

shown in Table 3.1. The CC2420 provides a digital received signal strength indicator (RSSI) value and a link quality indicator (LQI) value defined below.

**Received Signal Strength Indicator (RSSI)** RSSI is a measurement of the power present in a received radio signal at the RF pins measured in dBm. It is a value in the range [-100,0] dBm. The RSSI associated with a specific packet can be accessed via the CC2420 right after packet reception.

**Link Quality Indicator (LQI)** On each packet reception, CC2420 samples the first eight chips, calculates the error rate and produces an LQI value associated with each received packet. LQI is a characterization of the strength or quality of a received packet. It lies in the range [0,255].

### Antenna

Tmote Sky has an onboard microstrip antenna. The radiation pattern of the antenna approximates an omnidirectional pattern although it is not perfect. Tmote Sky can also be reconfigured for an external antenna by an SMA connector. One of the nodes used in the experiments of this thesis has the SPIDA attached to it by an external SMA connector while the other nodes use the onboard microstrip antenna.

### Sensors

Tmote Sky contains sensors for temperature, humidity and light. The temperature/humidity sensor is the SHT module manufactured by Sensirion AG. It is produced using a CMOS process and is coupled with a 14-bit A/D converter. The details of the SHT sensor are available on its datasheet [3]. A variety of light sensors may be used with Tmote Sky. The most commonly used ones are photodiodes.

[3] http://www.sensirion.com

**External Flash**

Tmote Sky uses the ST M25P80 40MHz serial code flash for external data and code storage. The external flash holds 1024KB of data. It shares SPI communication lines with the CC2420 radio transceiver. Hence, care should be taken when reading or writing to the flash since it is interleaved with radio communication.

### 3.2.2 SPIDA

The SPIDA, which is originally developed by Nilsson at SICS and shown in Figure 2.8, is an electronically switched parasitic element (ESPE) antenna designed primarily for the 2.4 GHz ISM band [17]. It consists of a central monopole, surrounded by six monopole-like parasitic elements spaced approximately quarter-wavelength apart. The parasitic elements work as *reflectors* of radiated power when they are grounded and as *directors* of the power when they are isolated. Hence, the reactance between the elements is controlled. This is achieved by biasing a capacitance diode with a controlled DC voltage.

SPIDA is simple and inexpensive to manufacture. Its construction involves a small hexagonal disc made of copper-clad FR-4 circuit board, on which six legs made of 1-mm copper wire have been soldered [17]. An SMA connector, which helps to connect SPIDA with a Tmote Sky, is mounted centrally on the the disc. The SMA connector, which costs 5 ECU in single quantities, is the most expensive part of SPIDA.

The radiation pattern of SPIDA approximates an offset circle that varies between -7.4 dB and 4.27 dB in the azimuthal plane without any significant sidelobes as observed from simulations and experiments [17]. Nevertheless, there is an 11 dB (7 dB effective) gain difference between 0° and 180° directions [17].

Österöm et al. [18] design the electronic circuit that is used to control SPIDA. They also show the schematic of the circuit to control an individual parasitic element. The circuit has a built-in scheme to reduce interference and suppress noise entering the sensor node. The available I/O lines on the Tmote Sky are used to control the parasitic elements by using two LC filters for each input-output line to prevent noise from entering the RF section. Each parasitic element is controlled by an ADG902 SPST RF solid state switch. The control circuit is soldered onto a strip-board with an attached 10-pin IDC connector that fits onto the Tmote Sky expansion pins.

Österöm et al. [18] also design the software drivers used to control the six parasitic elements of the SPIDA. Contiki [10] is the targeted operating system in the design of the drivers. They provide an API to direct transmission in a specific direction. That API is used in this thesis during writing the experiment programs.

## 3.3 Software Design

In this thesis the program for the experiments are written using C and certain Contiki specific structures and function calls. Then the program is uploaded on all the nodes

involved in the experiments before conducting the actual experiments.

### 3.3.1 Contiki

Contiki [10] is a state-of-art, open source operating system for sensor networks and other network embedded devices developed at SICS. Contiki is the first operating system for sensor networks to provide TCP/IP communication, loadable modules, protocol independent radio networking, cross-layer network simulation, software-based power profiling and threading on top of its event-driven kernel. It can effectively be used to program the Tmote Sky nodes for specific experimental setups and aid communication between them.

### 3.3.2 Program for Experiments

The program for experiments are written and uploaded on all the nodes. One node equipped with SPIDA and located right at the center in front of all the others nodes serves as a *base* and 16 other nodes in a square grid serve as *probes*. The program for the experiments are written in such a way that the base node broadcasts packets and the probe nodes receive the packets sent from the base node, measure and compute metrics and send it back to the base node by a unicast message at the end of the experiment.

The following parameters are identified as the inputs and outputs of the program written for the experiments.

#### Inputs of the Program

Here the inputs within the program for the experiments and the corresponding available selections are described. The requirement in terms of selections to meet the objectives of the experiments is also pointed out.

**Configuration of SPIDA:** This corresponds to transmitting in any one of the six available directions. Any one of the six legs of SPIDA can be turned on with in the program for the experiments.

**Transmission power:** Any of the available values indicated in Table 3.1 can be used to set the transmission power of the base node. An appropriate value of the transmission power can be selected to detect the boundaries of the radiation pattern of the antenna for a given grid of nodes.

**Number of Packets:** This is the number of packets sent from the base node to the probe nodes. An appropriate number of packets can be selected to reduce the impact of temporary fluctuations that may arise in the radio environment.

**Inter-packet Time Interval:** This is the time interval between two packet transmissions. An appropriate interval can be set to make packets independent from each other and increase the time span of the experiments there by reducing the impact of temporary fluctuations that may arise in the radio environment.

**Slack Time:** This is a time used to delay the transmission of metrics from the probe nodes. This is done in order to make sure that the probe nodes send their metrics after the base node has finished sending the packets.

**Outputs of the Program (Probe Statistics)**

Here the outputs obtained after conducting an experiment based on the program for the experiments are described. The outputs of the program are called *probe statistics* since they are the values of the metrics measured at the probe nodes.

**Average RSSI:** This is the average of the RSSI of all the received packets at each probe node.

**Average LQI:** This is the average of the LQI of all the received packets at each probe node.

**Packet Reception Rate (PRR):** After counting the packets they receive, the probe nodes finally divide the number of received packets by the total number of packets sent from the base node returning their packet reception rate (PRR).

The following step-wise procedures are included inside the program for experiments in order to meet the objectives of the experiment and build the model.

1. One of the legs of the SPIDA is turned on the base node and broadcasts a start message notifying the number of packets the base node is going to send and the inter-packet time interval at the highest transmission power *i.e.* 31. This is done in order to make sure that all the probe nodes receive at least the start message.
2. Soon after all the probe nodes receive the start message, the base node broadcasts its packets periodically at a smaller power.
3. The probe nodes record the RSSI and LQI values of each received packet. They also count the number of packets each of them received which is used to calculate the packet reception rate (PRR) at each probe node.
4. The probe nodes then average the RSSI and LQI over all the received packets. They also calculate the PRR by dividing the number of packets they receive by the total number of packets sent by the base node. Hence, all the probe statistics needed are available at this stage.

5. After the base finishes sending its packets, the probes send their statistics by a unicast message addressed to the base node. The timing for the end of the sending phase of the base in this case is calculated by multiplying the inter-packet time interval with the number of packets sent and adding a slack time as a safeguard. Each probe node sends its statistics at a random time to avoid collisions between the packets sent by the probe nodes.

6. Finally the statistics are obtained from the base node by logging into it through the USB port and directing the output into a file in our laptop.

7. The probe nodes are reset at the end of each experiment in order to cancel statistics computed from a previously conducted experiment.

## 3.4 Setup of Experiments

Here the framework of the basic experimental setup is described. The selection of the environment and the placement of the nodes are discussed. Specific values are also chosen to be used as inputs of the experiment program as described in subsection 3.3.2.

### 3.4.1 Selection of Environment

The environment for the experiments is carefully selected. An environment that is free from obstacles as much as possible is selected. An open grass field where there are no surrounding buildings and people is selected. This is to remove the harmful effects of multipath fading. The selected environment is also free from sources of interference such as WiFi.

### 3.4.2 Placement of Nodes

All the nodes are strategically placed at different points in a two-dimensional space. The nodes are placed on card board pipes of height 106.7 cm to remove harmful effects contributing to multipath fading from ground reflections. The probe nodes are arranged in a square grid with the base right in front of the grid. The USB port of the probes faces towards the base in all experiments. Figure 3.2 shows real real pictures depicting the setup of the experiments when the distance between two adjacent probe nodes is 6m and the base node is 3m in front of the square grid. Figure 3.3 shows the schematics for the node placement used throughout the remaining parts of the thesis. In the schematics $d$ stands for the distances with in the square grid and $b$ stands for the distance from the center of the probe front to the base node.

### 3.4.3 Selection of Values for the Inputs in the Program for Experiments

Constant values are chosen for the total number of packets, the inter-packet time interval and the slack time in all experiments. The number of packets sent from the base node is 1000 . A slow inter-packet time interval of 500 ms is selected. A slack time

of 10s is used. Hence, the experiments are designed to span a significant amount of time to reduce the effect of temporary fluctuations in the environment to a large extent. Different values are used for the transmission power depending on the size of the grid and one of the six legs of the SPIDA is turned on depending on the interest from the specific experiment.

(a) All nodes

(b) Base node with a USB cable attached

(c) Probe nodes

Figure 3.2: Setup of experiments

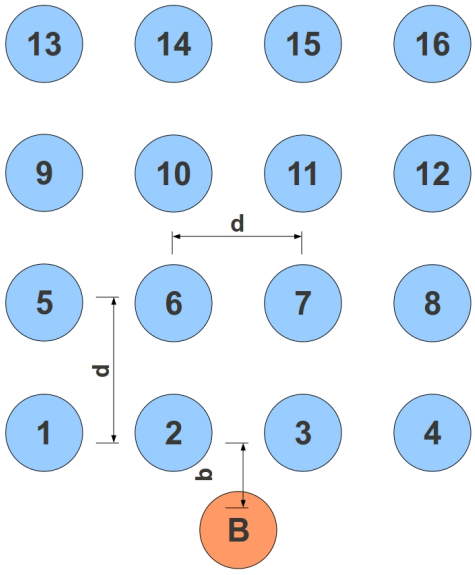


Figure 3.3: Schematics of the placement of nodes, 1-16:probe nodes, B:base node

# Chapter 4

# Experiments: Settings and Results

Here the details of the particular experimental settings are described and the results obtained are also presented. Several experiments are conducted at various settings. However, all the results from the different experimental settings are not presented to avoid redundancy and for the sake of brevity. Data from repetitions of two representative settings are presented. One of them is used for modeling purposes. Experiments are conducted with different grids, locations of the base, configurations of SPIDA and transmission power. Each particular setup is also repeated a number of times.

The experiments conducted can basically be categorized into two: *boundary experiments* and *granularity experiments*. The boundary experiments are conducted in order to observe the boundaries of the radiation pattern of SPIDA with in the grid considered. The granularity experiments are conducted to gather adequate data that can characterize the radiation pattern of SPIDA in a fine granular grid irrespective of its size. Experiments are conducted and data is collected from all the legs of the SPIDA in the granularity experiments.The transmission powers and the dimensions with in the grid are also varied to obtain a complete characterization of SPIDA in the granularity experiments.

## 4.1 Granularity Experiments

The main objective of the granularity experiments is to obtain a detail characterization of SPIDA without any interest on the boundaries of the radiation pattern. Experiments are performed in three different distance settings. Within each distance setting, the transmission power and configuration of SPIDA are varied. Figure 3.3 is used in referring to the setup. In all of these experiments, the transmission power is increased until no any significant changes in PRR is observed.

1. A distance setting where $d = 2m$, and $b = 2m$. Each of the six different legs of the SPIDA is turned on in different experiments. For each leg of SPIDA turned

on, transmission powers 2, 3, 5, 7 and 9 are used in successive sub-experiments. Each sub-experiment is repeated 10 times.

2. A distance setting where $d = 3m$, and $b = 3m$. Each of the six different legs of the SPIDA is turend on in different experiments. For each leg of SPIDA turned on, transmission powers 2, 3, 5, 7, 9 and 11 are used in successive sub-experiments. Each sub-experiment is repeated 10 times.

3. A distance setting where $d = 4m$, and $b = 4m$. Each of the six different legs of the SPIDA is turend on in different experiments. For each leg of SPIDA turned on, transmission powers 2, 3, 5, 7, 9, 11 and 15 are used in successive sub-experiments. Each sub-experiment is repeated 10 times.

Figure 4.1 shows a summary of the data collected from the experiments of the first type when leg 1 of SPIDA is turned on facing perpendicular to the probe front and uses a transmission power of 5. It can be seen that for this particularly small grid all the probe nodes have received all packets sent except the one at position 4. It can also be seen that this particular node has the lowest average RSSI and LQI values. It also shows a larger variability in the metrics compared to the others nodes which show a very small variability. This shows that position 4 is not covered by the main radiation beam of SPIDA at this particular setting. The asymmetries in the data can also be observed. The asymmetries can be due to the imperfections in the SPIDA prototype construction, the twists and turns of the legs due to wear and tear, the imprecision in adjusting the SPIDA perpendicular to the grid and distance measurement inaccuracies. The effects of the variation of the operating voltage of the Tmote Sky sensor node when it is powered from battery can also be cited here as a cause of asymmetry since different nodes at symmetric locations may actually operate at different voltages.

## 4.2 Boundary Experiments

Here the interest is to observe the boundaries of the radiation pattern of SPIDA with in a square grid of probe nodes as shown in Figure 3.3. This is achieved by identifying positions where PRR is zero or very small. Three experiments with different settings are performed in these group as described below. Figure 3.3 is used in referring to the setup.

1. A transmission power of 3, SPIDA leg 1 on and facing probe nodes, $d = 3m$, and $b = 3m$. This experiment is repeated 10 times. The boundaries cannot be observed at this stage.

2. A transmission power of 3, SPIDA leg 1 on and facing probe nodes, $d = 4m$, and $b = 3m$. This experiment is repeated 10 times. Some pattern starts to emerge at this setting but it is not very clear and symmetrical.

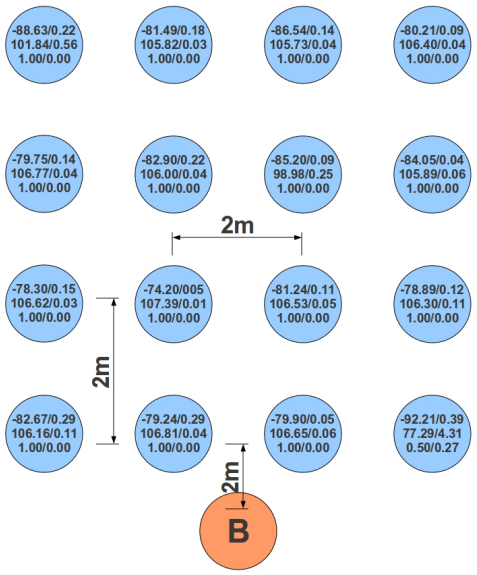


Figure 4.1: Summary of experiment data. First: RSSI, Second: LQI, Third: PRR Left: Averages, Right: Standard deviation

3. A transmission power of 3, SPIDA leg 1 on and facing probe nodes, $d = 6m$, and $b = 3m$. Now a pattern that shows the boundaries of the radiation pattern of SPIDA can be seen. This experiment is repeated 46 times. However, asymmetries are observed here too.

Figure 4.2 shows the raw data collected from the third experimental setting. The zeros at positions 8, 9, 11, 12, 13 and 16 show that there are no received packets at those positions for all the 46 repetitions. This data is used to build the model after performing certain compensations for the asymmetries as described in Chapter 5.

The boundaries of the radiation beam from SPIDA and its directional behavior can be observed from Figure 4.2. All the probe nodes on the left and right margins other than 1, 4 and 5 have a PRR of 0. The PRR of 1, 4 and 5 is also very small and close to zero. Probe nodes 14 and 15 receive packets due to the directional behavior of SPIDA and since they lie inside the radiation beam. There is a hole in PRR at position 11. This can be due the imperfections and imprecisions described above in subsection 4.2.

Another thing that can be observed from Figure 4.2 is that the standard deviation of PRR is larger than the mean at positions 1, 4 and 14. In statistics, this shows a vari-

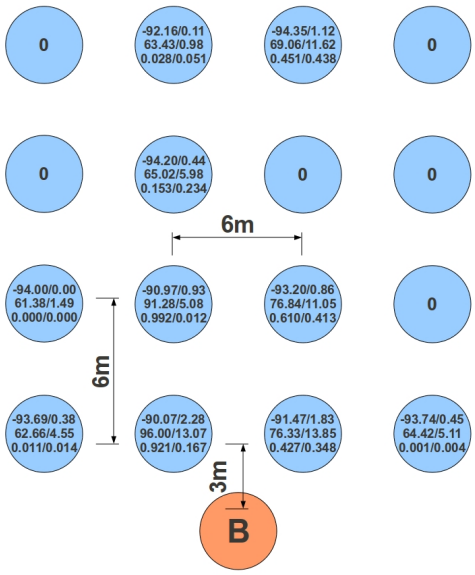


Figure 4.2: Summary of raw data. First: RSSI, Second: LQI, Third: PRR Left: Averages, Right: Standard deviation

ability in the data which suggests that the data has to be reconsidered and evaluated for further investigation. But in this case the cause for the high variability is understandable. In certain nodes, even though there is a large variability in PRR, the maximum value from the repetitions is still very small compared to the maximum possible value. Another cause of the variability is that a slight movement in the base can cause the radiation beam of SPIDA to cover or uncover positions which are close to the boundary of the beam. This can also cause a large variability in PRR among the several repetitions taken over a course of time.

# Chapter 5

# Modeling

A model that describes the temporal and spatial characteristics of the probe statistics considered is built. The probabilistic model gives the values of the signal strength and packet reception rate from a base node equipped with SPIDA at a certain point as outputs given the two-dimensional distance coordinates of the point and the configuration of SPIDA as inputs.

## 5.1 Model Buildup

Three major problems are basically observed in the process of building the model:

- the asymmetries in the measured metrics
- temporal variations in the measured metrics
- large spread distance between the points where we measure the metrics giving rise to a large spatial variation in the measured metrics

A simple yet effective way is used to compensate for the asymmetries. Random variable theory is used basically to study the temporal variation of the metrics considered. The methods from random variable theory also account for the imperfections and imprecisions that affect the values of the measured metrics. A suitable two-dimensional spatial interpolation mechanism is used to add fictitious points between the real points and estimate the values of the metrics at these points thus obtaining data at many more points than the ones actually existing in the network.

### 5.1.1 Compensation for Asymmetries and Assumptions

Before presenting the sample model data, a compensation for the asymmetries observed in the raw probe statistics data in Figure 4.2 is performed. The asymmetries are compensated by flipping half of the data collected from the 46 repetitions to the

opposite side along a line across the center of the square grid of probe nodes. For example after considering data from the first 23 repetitions for position 1, the remaining 23 repetitions are taken from the data collected for position 4 and vice versa.

After performing the compensation, the mean and standard deviations of the probe statistics are computed at the different positions. During some repetitions of the experiments, there are no received packets at certain positions. Hence the RSSI and LQI values are not obtained during those repetitions as indicated in the raw data. The minimum values observed in the experiments for RSSI and LQI are assumed at those points for consistency in computations and further modeling. These values are -96.13 for RSSI, and 48 for LQI. Figure 5.1 summarizes the compensated data gathered from the 46 repetitions at the different positions.

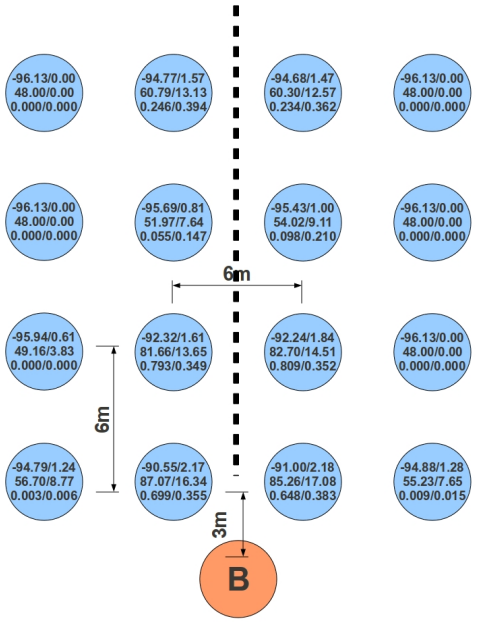


Figure 5.1: Summary of compensated data. First: RSSI, Second: LQI, Third: PRR Left: Averages, Right: Standard deviation

The boundaries of the radiation beam from SPIDA and its directional behavior can be observed in Figure 5.1. All the probe nodes on the left and right margins other than 1 and 4 have a PRR of 0. The PRR of 1 and 4 is also very small. Probes 14 and 15 receive some packets though small due to the directional behavior of SPIDA and since they lie inside the radiation beam. It can also be seen that the simple compensation technique

is effective and resulted in an approximately symmetrical pattern of the radiation beam of the SPIDA.

### 5.1.2 Temporal Modeling

The temporal variations observed in the metrics are accounted by constructing a probability density function (PDF) for each of the metrics at the different positions. A probabilistic model that provides the possible values of RSSI and PRR with certain probabilities at the 16 different probe positions in Figure 3.3 is first built. The model is built after performing a compensation on the original temporal random data obtained from all the 46 repetitions that is presented and summarized in Figure 4.2. The data is gathered from the final setup described in section 4: 6m grid, base node 3m away and SPIDA leg 1 turned on perpendicular to the probe front, and transmission power 3. The steps followed in building the mode are described below. Programs and functions are written in MATLAB and the Statistical Toolbox of MATLAB is used for the different steps involved in the model buildup.

1. The PDF for the probe statistics at each position is estimated from the collected random data in the repetitions using kernel density estimation from the non-parametric methods of density estimation which is used for a relate problem in WSNs using omnidirectional antennas [6].

2. A fine stepwise set of the values of the probe statistics is generated and the values of the PDF at these points is obtained.

3. The probabilities that the probe statistics lie between two consecutive values are evaluated from the area covered by the PDF between the two consecutive values.

4. A table is constructed for each of the 16 positions showing the stepwise set of values on one column and the probabilities that the probe statistics lie between two consecutive values on the other column. The validity of the probabilities is cross-checked by adding them. The probabilities add up to a number close to unity which is the expected value in a random experiment with mutually exclusive outcomes.

### 5.1.3 Spatial Modeling

Next the interest is to model the spatial characteristics of the probe statistics in the two-dimensional grid considered. Additional 33 new points are obtained with in the original grid by overlaying a grid using lines drawn halfway between lines in the original grid where probe nodes are located. The new points are labeled from *a-z* and then *A-G* as shown in Figure 5.2. Hence, the total number of points is 49: 16 original points and 33 fictitious points. Bilinear interpolation is used on the data from each repetition at the 16 points to compute the value of the probe statistics at the 33 fictitious points. This provides an estimation of the probe statistics from 46 repetitions at several points with in the original grid. Then the same steps that we have applied on the original data to construct the tables for the fictitious points are applied for the fictitious points.

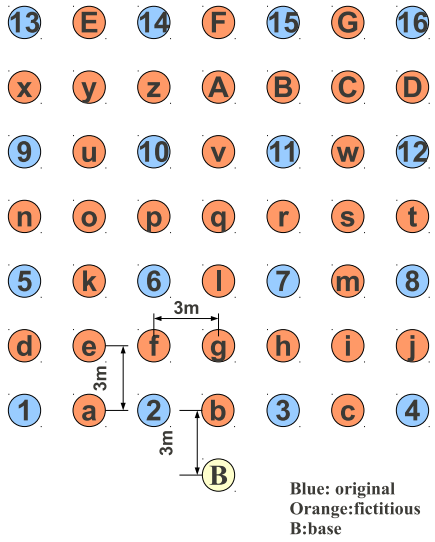


Figure 5.2: Original points and fictitious points. 1-16:original, a-z/A-G:fictitious

## 5.2 Sample Model Data

Here the PDFs and the probability tables for certain selected original and fictitious positions within the grid are shown. Certain representative positions within the grid are selected. Position 1 is close to the boundary of the radiation beam of SPIDA. Position *a* lies between the boundary and position 2 which is covered by the beam of SPIDA. Position 7 lies around the center of the beam.

Figure 5.3 shows the PDF of RSSI and PRR for position 1 while Table 5.1 shows the table of probabilities for RSSI and PRR.

Two peaks can be observed in the PDF of the RSSI: one around -96 and another one around -93.5. The one around -96 shows the several instances of the repetitions where there are no received packets at position 1. This is because position 1 is around the boundary of the radiation beam of SPIDA and it can easily be covered or uncovered by the radiation beam. This can also be observed from the PDF of the PRR. It can actually be seen that position 1 is not likely to have a PRR greater than 0.005. The last row in the second column of all probability tables is also empty since the probabilities are computed between two values of the probe statistics.

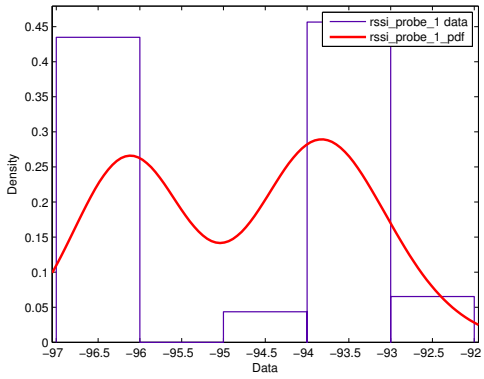


(a) PDF for RSSI at position 1

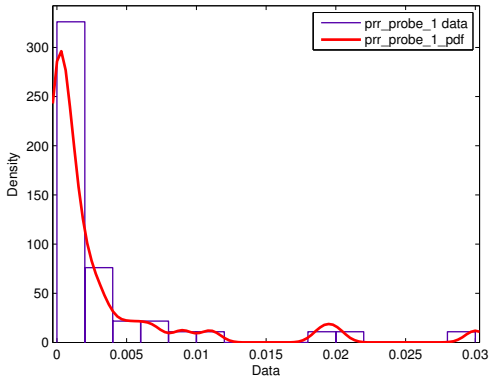


(b) PDF for PRR at position 1

Figure 5.3: PDF of probe statistics at position 1

(a) Table of probabilities for RSSI at position 1

| RSSI | Probability |
|---|---|
| -97.50 | 0.0238 |
| -97.10 | 0.0540 |
| -96.70 | 0.0875 |
| -96.30 | 0.1020 |
| -95.90 | 0.0885 |
| -95.50 | 0.0662 |
| -95.10 | 0.0623 |
| -94.70 | 0.0819 |
| -94.30 | 0.1058 |
| -93.90 | 0.1107 |
| -93.50 | 0.0912 |
| -93.10 | 0.0603 |
| -92.70 | 0.0330 |
| -92.30 | 0.0152 |
| -91.90 | 0.0059 |
| -91.50 | 0.0019 |
| -91.10 | |

(b) Table of probabilities for PRR at position 1

| PRR | Probability |
|---|---|
| 0.000 | 0.6954 |
| 0.002 | 0.1457 |
| 0.004 | 0.0534 |
| 0.006 | 0.0311 |
| 0.008 | 0.0189 |
| 0.010 | 0.0140 |
| 0.012 | 0.0047 |
| 0.014 | 0.0000 |
| 0.016 | 0.0049 |
| 0.018 | 0.0215 |
| 0.020 | 0.0168 |
| 0.022 | 0.0003 |
| 0.024 | 0.0000 |
| 0.026 | 0.0003 |
| 0.028 | 0.0122 |
| 0.030 | 0.0122 |
| 0.032 | 0.0003 |
| 0.034 | |

Table 5.1: Table of probabilities for probe statistics at position 1

Now the PDFs and the probability tables for the fictitious position *a* are shown. Figure 5.4 shows the PDF of RSSI and PRR for position *a* while Table 5.2 shows the table of probabilities for RSSI and PRR.

The PDF of the PRR at position *a* shows two peaks. This is due to the measurement of two distinct sets of PRRs with a significant difference at that point, showing a large variability in the PRR. This is interesting to see since position *a* is a fictitious point lying between a point around the boundary of the radiation beam and a point inside the radiation beam. The two peaks in turn show the likelihood that this point can belong to one of these regions.

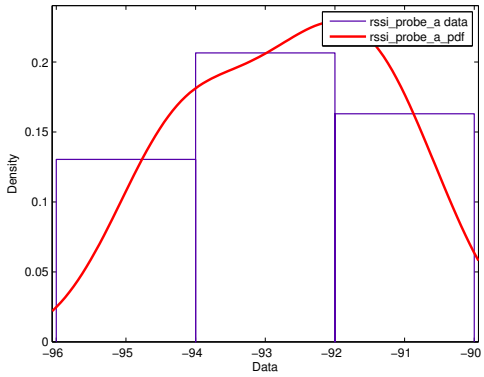


(a) PDF for RSSI at position *a*

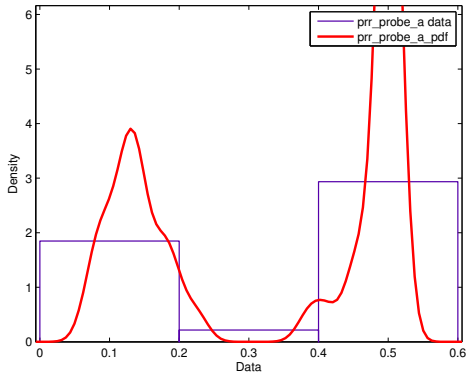


(b) PDF for PRR at position *a*

Figure 5.4: PDF of probe statistics at position *a*

(a) Table of probabilities for RSSI at position *a*

| RSSI | Probability |
|---|---|
| -97.00 | 0.0024 |
| -96.50 | 0.0082 |
| -96.00 | 0.0210 |
| -95.50 | 0.0417 |
| -95.00 | 0.0653 |
| -94.50 | 0.0837 |
| -94.00 | 0.0939 |
| -93.50 | 0.1001 |
| -93.00 | 0.1067 |
| -92.50 | 0.1124 |
| -92.00 | 0.1114 |
| -91.50 | 0.0984 |
| -91.00 | 0.0740 |
| -90.50 | 0.0457 |
| -90.00 | 0.0225 |
| -89.50 | 0.0087 |
| -89.00 | 0.0026 |
| -88.50 | 0.0006 |
| -88.00 | |

(b) Table of probabilities for PRR at position *a*

| PRR | Probability |
|---|---|
| 0.000 | 0.0004 |
| 0.030 | 0.0123 |
| 0.060 | 0.0469 |
| 0.090 | 0.0892 |
| 0.120 | 0.0996 |
| 0.150 | 0.0744 |
| 0.180 | 0.434 |
| 0.210 | 0.0195 |
| 0.240 | 0.0054 |
| 0.270 | 0.0002 |
| 0.300 | 0.0000 |
| 0.330 | 0.0023 |
| 0.360 | 0.0128 |
| 0.390 | 0.0215 |
| 0.420 | 0.0347 |
| 0.450 | 0.1145 |
| 0.480 | 0.2426 |
| 0.510 | 0.1659 |
| 0.540 | 0.0140 |
| 0.570 | 0.0001 |
| 0.600 | |

Table 5.2: Table of probabilities for probe statistics at position *a*

Here the PDFs and the probability tables for position 7 are shown. Figure 5.5 shows the PDF of RSSI and PRR for position 6 while Table 5.3 shows the table of probabilities for RSSI and PRR.

From the PDF for PRR and the probability table at position 7, it can be observed that the PRR at that position is likely to be close to unity except some rare instances which cause large variability. This is because of the reason that position 7 is located right in the centre of the radiation beam of SPIDA. The same reasoning also applies for the observation of a smooth variation in the PDF of RSSI at position 7.

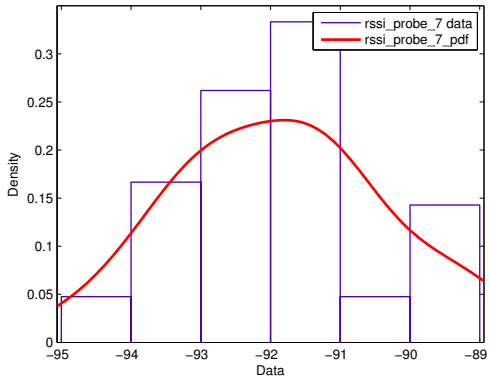


(a) PDF for RSSI at position 7

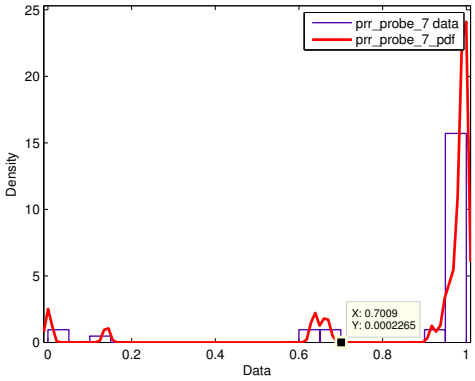


(b) PDF for PRR at position 7

Figure 5.5: PDF of probe statistics at position 7

(a) Table of probabilities for RSSI at position 7

| RSSI | Probability |
|---|---|
| -96.00 | 0.0076 |
| -95.50 | 0.0154 |
| -95.00 | 0.0279 |
| -94.50 | 0.0462 |
| -94.00 | 0.0687 |
| -93.50 | 0.0902 |
| -93.00 | 0.1051 |
| -92.50 | 0.1127 |
| -92.00 | 0.1144 |
| -91.50 | 0.1074 |
| -91.00 | 0.0899 |
| -90.50 | 0.0685 |
| -90.00 | 0.0517 |
| -89.50 | 0.0392 |
| -89.00 | 0.0269 |
| -88.50 | 0.0148 |
| -88.00 | 0.0062 |
| -87.50 | 0.0019 |
| -87.00 | 0.0004 |
| -86.50 | 0.0001 |
| -86.00 | |

(b) Table of probabilities for PRR at position 7

| PRR | Probability |
|---|---|
| 0.000 | 0.0519 |
| 0.020 | 0.0012 |
| 0.040 | 0.0000 |
| 0.100 | 0.0003 |
| 0.120 | 0.0131 |
| 0.140 | 0.0131 |
| 0.160 | 0.0003 |
| 0.180 | 0.0000 |
| 0.600 | 0.0031 |
| 0.620 | 0.0246 |
| 0.640 | 0.0397 |
| 0.660 | 0.0236 |
| 0.680 | 0.0054 |
| 0.700 | 0.0000 |
| 0.880 | 0.0005 |
| 0.900 | 0.0133 |
| 0.920 | 0.0290 |
| 0.940 | 0.0592 |
| 0.960 | 0.1583 |
| 0.980 | 0.5949 |
| 1.000 | |

Table 5.3: Table of probabilities for probe statistics at position 7

## 5.3 Model Use

The tables constructed as part of the model can be integrated with existing WSN simulators. From the tables, the ranges of the values that probe statistics lie with a specific probability at a given position is known. To measure the value of a metric at a specific position from an experiment conducted in a simulator, one can start by specifying the different ranges of values a specific metric can assume at a specific position. Then the outcomes of a certain experiment which results in a specific value of a metric at that position can be skewed to lie in one of the possible ranges according to the values given

in the probabilities column. Figure 5.6 depicts the inputs and outputs of the model of SPIDA developed in this thesis. The inputs to the model are the two-dimensional distance coordinates of a point in a space around a node equipped with SPIDA and the configuration of the SPIDA and the outputs of the model are the values of the signal strength and packet reception rate from the node at that particular point

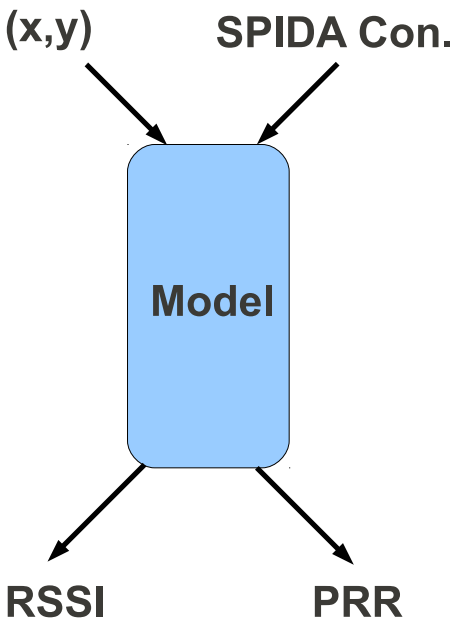


Figure 5.6: Model of SPIDA for WSNs

# Chapter 6

# Conclusion and Future work

In this thesis, a model of an electronically switchable directional antenna, SPIDA, for WSNs is built based on real-world experiments. A probabilistic model that accounts for temporal variations in metrics and inaccuracies and imprecisions affecting real-world experiments is built. Spatial variations are also considered with a suitable two-dimensional interpolation mechanism. Several experiments are conducted on different experimental settings before starting to build a model to obtain the representative setting that can be used to build a more accurate model.

The model is built based on an appropriate setup that shows the important directional properties of SPIDA. The programs for the experiments are designed to last for a longer duration and to take account of temporary fluctuations that may arise during an experiment. The environment for the experiments is carefully selected to reduce the harmful effects of multipath fading and interference. Thorough effort has been invested in trying to build a more accurate model in all aspects.

For the future, the model can be integrated into existing WSN simulators such as COOJA which is developed at SICS. The integration of the model into WSN simulators opens up many further opportunities for future works and researches that make use of the directional characteristics of SPIDA with a reduction in power consumption. The development of MAC and routing protocols for WSNs using SPIDA can possibly be one direction. Another direction can be developing localization and neighbor discovery algorithms in a WSN with SPIDA.

# Bibliography


[1] IEEE Std. 291-1991. IEEE standard methods for measuring electromagnetic field strength of sinusoidal continuous waves, 30Hz to 30GHz.

[2] I. Akyildiz, W. Su, Y. Sankarasubramaniam, and E. Cayirci. A survey on sensor networks. *IEEE Communication Mag.*, 40(8), 2002.

[3] Constantine A. Balanis. *Antenna Theory Analysis and Design*. John Wiley&Sons, third edition, 2005.

[4] Christopher M. Bishop. *Neural Networks for Pattern Recognition*. Clarendon Press, 1995.

[5] J. Redi C. Santivanez. On the use of directional antennas for sensor networks. In *Military Communications Conference (MILCOM 2003)*, 2003.

[6] Alberto Cerpa, Jennifer L. Wong, Louane Kuang, Miodrag Potkonjak, and Deborah Estrin. Statistical model of lossy links in wireless sensor networks. In *IPSN '05: Proceedings of the 4th International Symposium on Information Processing in Sensor Networks*, page 11, Piscataway, NJ, USA, 2005. IEEE Press.

[7] P. Chandra, M. Dobkin, A. Bensky, R. Olexa, A. Lide, and F. Dowla. *Wireless Networking*. Newnes, 2007.

[8] J. Cho, J. Lee, T. Kwon, and Y. Choi. Directional antenna at sink (DAaS) to prolong network lifetime in wireless sensor networks. In *Proc. of the European Wireless Conf. - Enabling Technologies for Wireless Multimedia Communications*, 2006.

[9] S. Cho and A. Chandrakasan. Energy efficient protocols for low duty cycle wireless microsensor. In *Proc. of the* $33^{rd}$ *Annual Hawaii International Conference on System Sciences*, volume 2, 2000.

[10] A. Dunkels, B. Grönvall, and T. Voigt. Contiki - A lightweight and flexible operating system for tiny networked sensors. In *Proc. of* $1^{st}$ *Wkshp. on Embedded Networked Sensors*, 2004.

[11] J. Dunlop and J. Cortes. Impact of directional antennas in wireless sensor networks. In *Proc. of the the* $4^{th}$ *Int. Conf. on Mobile Ad-Hoc and Sensor Systems (MASS)*, 2007.

[12] J. Dunlop and J. Cortes. Co-design of efficient contention mac with directional antennas in wireless sensor networks. In *Proc. of the International Wireless Communications and Mobile Computing Conference*, 2008.

[13] G. Giorgetti, A. Cidronali, S. Gupta, and G. Manes. Exploiting low-cost directional antennas in 2.4 GHz IEEE 802.15.4 wireless sensor networks. In *Proc. of the European Conf. on Wireless Technologies*, 2007.

[14] Frank B. Gross. *Smart Antennas for Wireless Communications*. McGraw-Hill, 2005.

[15] C. Intanagonwiwat, R. Govindan, D. Estrin, J. Heidemann, and F. Silva. Directed Diffusion for wireless sensor networking. *IEEE/ACM Trans. Networking*, 11(1), 2003.

[16] J.M. Kahn, R.H. Katz, and K.S.J. Pister. Next century challanges: Mobile networking for smart dust. In *Proc. of the ACM MobiCom'99*, 1999.

[17] M. Nilsson. Directional antennas for wireless sensor networks. In *Proc. of the* $9^{th}$ *Scandinavian Workshop on Wireless Adhoc Networks (Adhoc)*, 2009.

[18] Erik Öström, Luca Mottola, and Thiemo Voigt. Evaluation of an Electronically Switched Directional Antenna for Real-world Low-power Wireless Networks. In *4th International Workshop on Real-world Wireless Sensor Networks (REALWSN)*, 2010.

[19] Ph.D. Peyton Z. Peebles, Jr. *Probability, Random Variables, and Random Signal Principles*. McGraw Hill, fourth edition, 2002.

[20] G. J. Pottie and W. J. Kaiser. Wireless integrated network sensors. *Commun. ACM*, 43(5):51–58, 2000.

[21] Richard E. Woods Rafael C. Gonzalez. *Digital Image Processing*. Prentice Hall, second edition, 2002.

[22] E. Shihab, L. Cai, and J. Pan. A distributed, asynchronous directional-to-directional MAC protocol for wireless ad hoc networks. *IEEE Trans. on Vehicular Technology*, 58(9), 2009.

[23] William Stallings. *Wireless Communications and Networks*. Pearson Prentice Hall, 2005.

[24] Geoffrey Werner-allen, Jeff Johnson, Mario Ruiz, Jonathan Lees, and Matt Welsh. Monitoring volcanic eruptions with a wireless sensor network. In *in Proceedings of the Second European Workshop on Wireless Sensor Networks (EWSN05)*, 2005.

[25] Y. Wu, L. Zhang, Y. Wu, and Z. Niu. Interest dissemination with directional antennas for wireless sensor networks with mobile sinks. In *Proc. of the* $6^{th}$ *Int. Conf. on Embedded Networked Sensor Systems (SenSys)*, 2006.

[26] Carmen M. Yago and Pedro M. Ruiz. Energy-efficient multicast with directional antennae and localized tree reconfiguration. In *MSWiM '06: Proceedings of the 9th ACM international symposium on Modeling analysis and simulation of wireless and mobile systems*, pages 151–154, New York, NY, USA, 2006. ACM.

[27] Jennifer Yick, Biswanath Mukherjee, and Dipak Ghosal. Wireless sensor network survey. *Computer Networks*, 52(12):2292 – 2330, 2008.